# Performance analysis of surface plasmon resonance sensor with high-order absentee layer*

Qing-Qing Meng(孟庆卿)[1], Xin Zhao(赵鑫)[1], Shu-Jing Chen(陈淑静)[2], Cheng-You Lin(林承友)[1,†], Ying-Chun Ding(丁迎春)[1], and Zhao-Yang Chen(陈朝阳)[1,‡]

[1] College of Science, Beijing University of Chemical Technology, Beijing 100029, China

[2] Beijing Key Laboratory of Materials Utilization of Nonmetallic Minerals and Solid Wastes, National Laboratory of Mineral Materials, School of Materials Science and Technology, China University of Geosciences, Beijing 100083, China

(Received 3 July 2017; revised manuscript received 17 August 2017; published online 20 November 2017)

A surface plasmon resonance (SPR) sensor with a high-order absentee layer on the top of metallic film is proposed. The performance of the SPR sensor with NaCl, MgO, $TiO_2$ or AlAs high-order absentee layer is analyzed theoretically. The results indicate that the sensitivity and the full width at half maximum of those SPR sensors decrease with the increasing of the order of absentee layer, but the variation of the figure of merit (FOM) depends on the refractive index of absentee layer. By improving the order of absentee layer with high-refractive-index, the FOM of the SPR sensor can be enhanced. The maximum value of FOM for the SPR sensor with high-order $TiO_2$ (or AlAs) absentee layer is 1.059% (or 2.587%) higher than the one with one-order absentee layer. It is believed the proposed SPR sensor with high-order absentee layer will be helpful for developing the high-performance SPR sensors.

**Keywords:** surface plasmon resonance sensor, high-order absentee layer, figure of merit

**PACS:** 42.81.Pa, 78.20.–e, 07.60.–j **DOI:** 10.1088/1674-1056/26/12/124213

## 1. Introduction

As a valuable and standard analytical tool, surface plasmon resonance (SPR) sensors are widely used in gas molecule detection, drug diagnostics and biosensing,[1–3] and the spectral range of its application extends from visible and infrared bands to terahertz band now.[4–6] The Kretschmann prism coupling configuration is a simple and useful configuration of the SPR sensor. In this configuration, a high refractive index prism is coated with a thin metal layer touching the analyte (sensing medium).[7,8] When a p-polarized incident light illuminates on the SPR sensor, the surface plasmon wave (SPW) will occur at the interface between metal layer and analyte if the phase matching condition is satisfied.[9] The resonant condition is generally controlled by the incident angle or wavelength of the excitation light, which is usually referred to as the angular or wavelength interrogation. Under the phase matching condition, the electromagnetic field of the SPW becomes strongest when the energy of the light is completely absorbed, causing a sharp dip to appear on the reflectivity curve.[10,11]

To evaluate the performance of an SPR sensor, several performance parameters are generally used, such as the sensitivity ($S$), the full width at half maximum (FWHM), and the figure-of-merit (FOM).[2,11,12] The sensitivity is defined as the ratio between the shift of the resonance angle or wavelength and the change of the refractive index of analyte.[13] Many methods of improving the sensitivity were proposed recently, such as adding graphene and air gap,[14] dielectric layer[13,15] or semiconductor layer[16] in an SPR sensor. The FWHM of reflectance curve is another important parameter, which determines the detection accuracy of SPR sensor.[17] Exciting long-range surface plasmons by adding dielectric layer between the prism and metal layer was proven to be an efficient method to reduce the FWHM (or increase the detection accuracy).[18] The FOM is defined as the ratio between the sensitivity and the FWHM. It was demonstrated that the FOM can be enhanced by adding a thin dielectric layer with high refractive index on the top of the metallic layer in SPR sensor in the spectral interrogation.[19] In addition, using the liquid prism instead of the conventional solid prism was also verified for FOM enhancement.[11]

The absentee layer is an optical layer whose optical thickness satisfies the integer multiple of half-wavelength. Generally, the absentee layer has no effect on the reflectance or transmittance of the film system at the considered angle or wavelength, which is often used to adjust the spectral curve without changing the basic profile.[20,21] In our previous study,[22] a half-wavelength absentee layer was used in an SPR sensor for FOM enhancement. In this paper, we further investigate the performance of the SPR sensor with a high-order absentee layer.[23] By analyzing the sensitivity, FWHM and FOM

*Project supported by the National Natural Science Foundation of China (Grant Nos. 11547183 and 11547241), the Higher Education and High-quality and World-class Universities, China (Grant No. PY201612), the National Key Research and Development Program of China (Grant No. 2016YFB0302003), and the Natural Science Foundation of Beijing (Grant No. 2162033).

†Corresponding author. E-mail: cylin@mail.buct.edu.cn

‡Corresponding author. E-mail: chenzy@mail.buct.edu.cn

© 2017 Chinese Physical Society and IOP Publishing Ltd 

of the SPR sensor with different-order absentee layer, we find that the FOM of the SPR sensor can be enhanced by improving the order of high-refractive-index absentee layer.

## 2. Theory

### 2.1. Theory model

The SPR sensor with a high-order absentee layer is shown in Fig. 1(a). Compared with a traditional SPR sensor, the proposed SPR sensor contains a high-order absentee layer on the top of metal (gold) layer. A bi-layer model is used to analyze the performance of the proposed SPR sensor[24] as shown in Fig. 1(b). It is an accurate model because of the absence of approximation.[25] The bi-layer model of SPR sensor consists of an incident medium (the prism), a metal layer, a higher-order absentee layer and an emergent medium (the analyte).

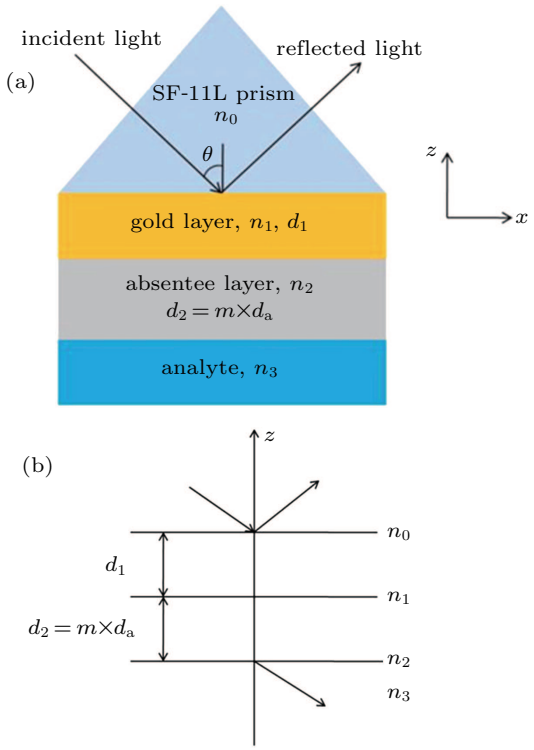



**Fig. 1.** (color online) (a) Schematic diagram and (b) bi-layer model of the SPR sensor with a high-order absentee layer.

### 2.2. Thin film theory

Based on the thin film theory, the tangential fields at the first (prism-metal layer) interface are related to those at the third (absentee layer-analyte) interface by

$$\begin{bmatrix} E_0 \\ H_0 \end{bmatrix} = \begin{bmatrix} \cos\delta_1 & \frac{\mathrm{i}}{\eta_1}\sin\delta_1 \\ \mathrm{i}\eta_1\sin\delta_1 & \cos\delta_1 \end{bmatrix} \times \begin{bmatrix} \cos\delta_2 & \frac{\mathrm{i}}{\eta_2}\sin\delta_2 \\ \mathrm{i}\eta_2\sin\delta_2 & \cos\delta_2 \end{bmatrix} \begin{bmatrix} E_3 \\ H_3 \end{bmatrix}, \quad (1)$$

where $\delta_1$ (or $\delta_2$) and $\eta_1$ (or $\eta_2$) are the phase factor and the optical admittance of the metal (or the high-order absentee layer), respectively; $\delta_i = 2\pi n_i d_i \cos\theta_i/\lambda$, with $n_i$ and $d_i$ representing the refractive index and layer thickness of each layer, respectively; $\lambda$ is the wavelength of incident light; $\theta_i$ is the refraction angle of light in each layer; $\eta_i = n_i/\cos\theta_i$ is applied to p-polarized light.

Because $H_3/E_3 = \eta_3$ and $H_1/E_1 = Y$, equation (1) can also be expressed as

$$E_1 \begin{bmatrix} 1 \\ Y \end{bmatrix} = \begin{bmatrix} \cos\delta_1 & \frac{i}{\eta_1}\sin\delta_1 \\ \mathrm{i}\eta_1\sin\delta_1 & \cos\delta_1 \end{bmatrix} \times \begin{bmatrix} \cos\delta_2 & \frac{i}{\eta_2}\sin\delta_2 \\ \mathrm{i}\eta_2\sin\delta_2 & \cos\delta_2 \end{bmatrix} \begin{bmatrix} 1 \\ \eta_3 \end{bmatrix} E_3. \quad (2)$$

So, the characteristic matrix of the bi-layer structure can be written as

$$\begin{bmatrix} B \\ C \end{bmatrix} = \begin{bmatrix} \cos\delta_1 & \frac{i}{\eta_1}\sin\delta_1 \\ \mathrm{i}\eta_1\sin\delta_1 & \cos\delta_1 \end{bmatrix} \times \begin{bmatrix} \cos\delta_2 & \frac{i}{\eta_2}\sin\delta_2 \\ \mathrm{i}\eta_2\sin\delta_2 & \cos\delta_2 \end{bmatrix} \begin{bmatrix} 1 \\ \eta_3 \end{bmatrix}. \quad (3)$$

The reflectance $R$ of the bi-layer structure can be derived by

$$R = \left| \frac{\eta_0 B - C}{\eta_0 B + C} \right|^2. \quad (4)$$

Using Eq. (4), the reflectance can be calculated as a function of incident angle (angular spectrum), and the performance parameters of the SPR sensor can be determined.

For an absentee layer, its optical thickness generally fulfills

$$n_2 d_2 \cos\theta_2 = m\frac{\lambda}{2}, \quad (m = 1, 2, \ldots). \quad (5)$$

In this paper, the absentee layer with $m = 1$ is called one-order absentee layer, and its thickness fulfills $d_a = \lambda/2n_2\cos\theta_2$. The absentee layer with $m > 1$ is named high-order absentee layer, and its thickness fulfills $d_2 = md_a$. The phase factor of an absentee layer $\delta_2 = m\pi$, and its characteristic matrix becomes a unity matrix at the target angle, which is

$$M_2 = \begin{bmatrix} \cos\delta_2 & \frac{\mathrm{i}}{\eta_2}\sin\delta_2 \\ \mathrm{i}\eta_2\sin\delta_2 & \cos\delta_2 \end{bmatrix} = \begin{bmatrix} \pm 1 & 0 \\ 0 & \pm 1 \end{bmatrix}. \quad (6)$$

Therefore, at the target angle, such as the resonance angle of a traditional SPR sensor, the extra reflections cancel out at the interfaces because no additional phase shifts are introduced. But at other incident angles, equations (5) and (6) are no longer fulfilled, leading to the change of reflectance. Overall, the adding of an absentee layer does not affect the reflectance of the SPR sensor at the resonance angle, but changes

the reflectance at other angles, which may be used to reduce the FWHM of the reflectance dip, and even increase the FOM of the SPR sensor without changing the resonance angle or the reflectance at the resonance angle.

### 2.3. Performance parameters

The performance of an SPR sensor can be described by several parameters, such as the resonance angle $\theta_{\rm res}$, depth of dip $R_{\rm res}$ (the reflectance at the resonance angle), sensitivity, FWHM, and FOM. In the angular interrogation mode, the resonance angle $\theta_{\rm res}$ changes with the refractive index of the analyte $n_{\rm s}$, so the sensitivity $S$ can be expressed as the ratio between the resonance angle variation $\Delta\theta_{\rm res}$ and the variation of refractive index of the analyte $\Delta n_{\rm s}$ as follows:

$$S = \frac{\Delta\theta_{\rm res}}{\Delta n_{\rm s}}. \tag{7}$$

The FWHM can be determined by calculating FWHM value of the reflectance dip ($\Delta\theta_{0.5}$), and expressed as

$$\text{FWHM} = \Delta\theta_{0.5}. \tag{8}$$

Thus the FOM can be calculated from

$$\text{FOM} = \frac{S}{\text{FWHM}}. \tag{9}$$

## 3. Result and discussion

Using the theoretical method described above, the performance of the SPR sensor with high-order absentee layer can be analyzed. The wavelength of the incident light is assumed to be 653.2 nm. A 45-degree SF-11L glass ($n_0 = 1.776$) is used as the prism material in SPR sensors. Gold (Au) ($n_1 = 0.166 + 3.15\text{i}$) film with an optimized thickness of 50 nm ($d_1 = 50$ nm) is employed as the metal film. The water ($n_3 = 1.33$) is assumed to be the analyte.

In addition, NaCl, MgO, $TiO_2$, and AlAs absentee layers are considered in our study, and their refractive indices are $n_{\rm NaCl} = 1.541$, $n_{\rm MgO} = 1.741$, $n_{\rm TiO_2} = 2.2789$, and $n_{\rm AlAs} = 3.112$, respectively. According to Eq. (5), the thickness values of one-order NaCl, MgO, $TiO_2$, and AlAs absentee layer ($d_{\rm a}$) are 695, 349, 187, and 119 nm respectively. All the data for the optical parameters of materials are cited from Refs. [26]–[28] and listed in Table 1.

**Table 1.** Refractive indices of materials at 653.2-nm wavelength of light.

| Material | Refractive index/RIU |
|---|---|
| Glass SF11 | 1.776 |
| Au | $0.166 + 3.15\text{i}$ |
| NaCl | 1.541 |
| MgO | 1.741 |
| $TiO_2$ | 2.2789 |
| AlAs | 3.112 |
| Water | 1.33 |

### 3.1. Performance of SPR sensors with high-order absentee layer

#### 3.1.1. NaCl absentee layer

Firstly, the performance of the SPR sensor with different-order NaCl absentee layer is studied. Figure 2 shows the reflectivity curves of SPR sensors with one-order, two-order, three-order, and four-order ($m = 1, 2, 3, 4$) NaCl absentee layer.

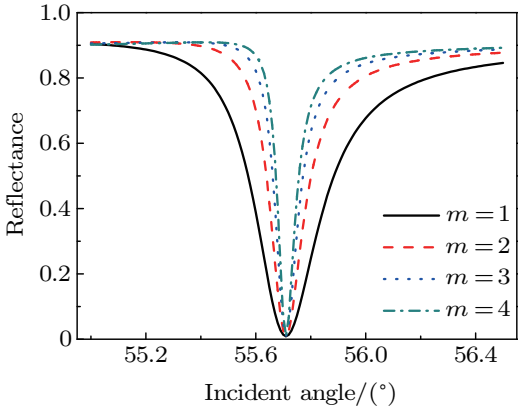



**Fig. 2.** (color online) Reflectivity curves of the SPR sensors with different-order NaCl absentee layer ($m = 1, 2, 3, 4$).

In Fig. 2, four reflectance curves show the same resonance angle and depth of dip (55.71° and 0.00927), because the absentee layer with different orders does not change the reflectance at the resonance angle. However, the FWHMs of reflectance curves are totally different from each other. With the increasing of the order of absentee layer ($m$), the reflectance dip becomes narrow, which means that the FWHM decreases. In Table 2, we list the performance parameters of these SPR sensors. For sensitivity calculation, the refractive index of analyte is assumed to be changed from 1.325 to 1.335.

**Table 2.** Performance parameters of the SPR sensors with different-order NaCl absentee layer ($m = 1, 2, 3, 4$).

| Order of absentee layer | Sensitivity/[(°)/RIU] | FWHM/(°) | FOM/RIU$^{-1}$ |
|---|---|---|---|
| $m = 1$ | 5.4 | 0.313 | 17.246 |
| $m = 2$ | 2.8 | 0.163 | 17.203 |
| $m = 3$ | 1.9 | 0.110 | 17.186 |
| $m = 4$ | 1.4 | 0.083 | 17.178 |

When $m$ increases from 1 to 4, the sensitivity decreases from 5.4°/RIU to 1.4°/RIU, and the FWHM also decreases from 0.313° to 0.083°. Consequently, the FOM decreases from 17.246 RIU$^{-1}$ to 17.178 RIU$^{-1}$. The decreasing of the FOM should be due to larger decrease rate of the sensitivity than that of the FWHM as $m$ increases. Compared with the SPR sensor with one-order absentee layer, the SPR sensor with high-order NaCl absentee layer can obtain small FWHM, but low sensitivity and FOM.

### 3.1.2. MgO absentee layer

Secondly, the performance of the SPR sensor with different-order MgO absentee layer is investigated. Figure 3 shows the reflectivity curves of SPR sensors with one-order, two-order, three-order, four-order ($m = 1, 2, 3, 4$) MgO absentee layer. Like Fig. 2, four reflectance curves in Fig. 3 still exhibit the same resonance angle and depth of dip. In addition, with the increasing of the order of absentee layer ($m$), the reflectance dip also becomes narrow. The performance parameters of these SPR sensors are listed in Table 3.

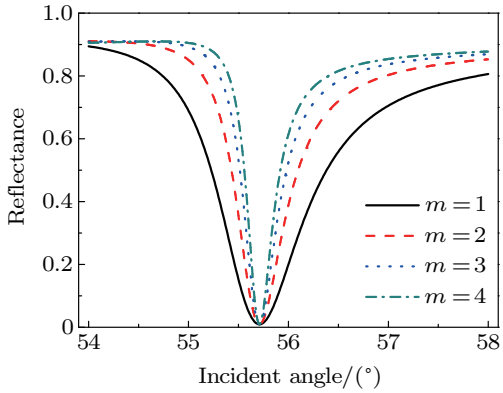



**Fig. 3.** (color online) Reflectivity curves of the SPR sensors with different-order MgO absentee layer ($m = 1, 2, 3, 4$).

As $m$ increases from 1 to 4, the sensitivity decreases from 19.7°/RIU to 6.1°/RIU, and the FWHM also decreases from 1.155° to 0.361°. Thus, the FOM decreases from 17.053 RIU$^{-1}$ to 17.038 RIU$^{-1}$. The decreasing of the FOM comes from larger decrease rate of the sensitivity than that of the FWHM as $m$ increases. Although the SPR sensor with high-order MgO absentee layer can achieve smaller FWHM than that with one-order absentee layer, it cannot obtain the larger FOM.

**Table 3.** Performance parameters of the SPR sensors with different-order MgO absentee layer ($m = 1, 2, 3, 4$).

| Order of absentee layer | Sensitivity/[(°)/RIU] | FWHM/(°) | FOM/RIU$^{-1}$ |
|---|---|---|---|
| $m = 1$ | 19.7 | 1.155 | 17.053 |
| $m = 2$ | 11.3 | 0.666 | 17.050 |
| $m = 3$ | 8.0 | 0.468 | 17.043 |
| $m = 4$ | 6.1 | 0.361 | 17.038 |

### 3.1.3. $TiO_2$ absentee layer

Next, the performance of the SPR sensor with different-order $TiO_2$ absentee layer is studied. Figure 4 shows the reflectivity curves of the SPR sensors with one-order, two-order, three-order, four-order ($m = 1, 2, 3, 4$) $TiO_2$ absentee layer. The performance parameters of these SPR sensors are listed in Table 4.

In Fig. 4, the resonance angles and depths of dip of all the four reflectance curves stay unchanged. When $m$ increases from 1 to 4, the sensitivity decreases from 41.4°/RIU to 17.8°/RIU, and the FWHM also decreases from 2.463° to 1.048°; however, the FOM does not decrease but increases from 16.819 RIU$^{-1}$ to 16.973 RIU$^{-1}$. The reason for the increasing of the FOM is attributed to the smaller decrease rate of the sensitivity than that of the FWHM as $m$ increases. So, compared with the SPR sensor with one-order absentee layer, the SPR sensor with high-order $TiO_2$ absentee layer can realize small FWHM and large FOM simultaneously.

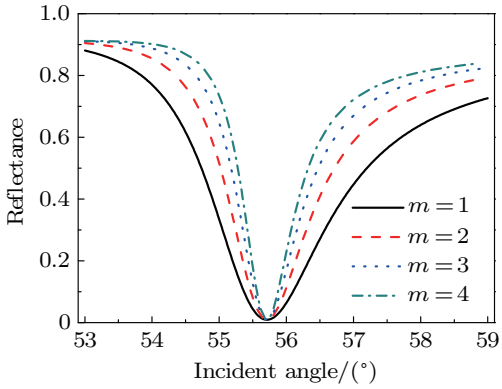



**Fig. 4.** (color online) Reflectivity curves of SPR sensors with different-order $TiO_2$ absentee layer ($m = 1, 2, 3, 4$).

**Table 4.** Performance parameters of the SPR sensors with different-order $TiO_2$ absentee layer ($m = 1, 2, 3, 4$).

| Order of absentee layer | Sensitivity/[(°)/RIU] | FWHM/(°) | FOM/RIU$^{-1}$ |
|---|---|---|---|
| $m = 1$ | 41.4 | 2.463 | 16.809 |
| $m = 2$ | 28.7 | 1.696 | 16.922 |
| $m = 3$ | 22.0 | 1.295 | 16.988 |
| $m = 4$ | 17.8 | 1.048 | 16.985 |

### 3.1.4. AlAs absentee layer

Finally, the performance of the SPR sensors with different-order AlAs absentee layer is investigated. Fig. 5 shows the reflectivity curves of the SPR sensors with one-order, two-order, three-order, four-order ($m = 1, 2, 3, 4$) AlAs absentee layer. The performance parameters of these SPR sensors are listed in Table 5.

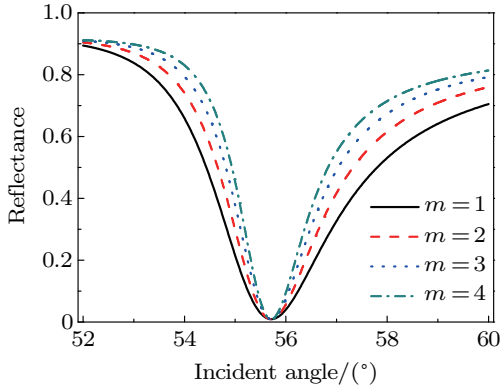



**Fig. 5.** (color online) Reflectivity curves of SPR sensors with different-order AlAs absentee layer ($m = 1, 2, 3, 4$).

**Table 5.** Performance parameters of SPR sensors with different-order AlAs absentee layer ($m = 1, 2, 3, 4$).

| Order of absentee layer | Sensitivity/[(°)/RIU] | FWHM/° | FOM/RIU$^{-1}$ |
|---|---|---|---|
| $m = 1$ | 56.0 | 3.372 | 16.619 |
| $m = 2$ | 44.9 | 2.671 | 16.817 |
| $m = 3$ | 37.5 | 2.217 | 16.906 |
| $m = 4$ | 32.2 | 1.897 | 16.953 |

The sensitivity decreases from 56.0 to 32.2°/RIU, and the FWHM decreases from 3.372° to 1.897° as $m$ increases from 1 to 4. Like the case of AlAs absentee layer, the FOM also increases, in this case, from 16.619 RIU$^{-1}$ to 16.953 RIU$^{-1}$. The reason for the increasing of the FOM should be attributed to the smaller decrease rate of the sensitivity than that of the FWHM as $m$ increases. Compared with the SPR sensor with one-order absentee layer, the SPR sensor with high-order AlAs absentee layer can also realize small FWHM and large FOM simultaneously.

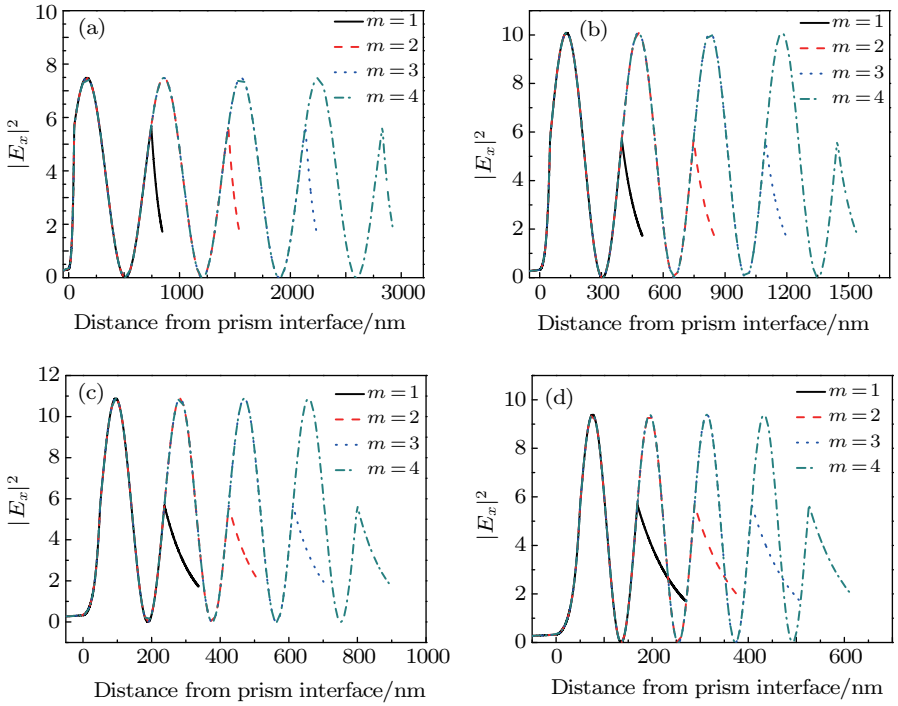



**Fig. 6.** (color online) Distributions of $|E_x|^2$ of SPR sensors with different-order ($m = 1, 2, 3, 4$) (a) NaCl, (b) MgO, (c) $TiO_2$, and (d) AlAs absentee layer.

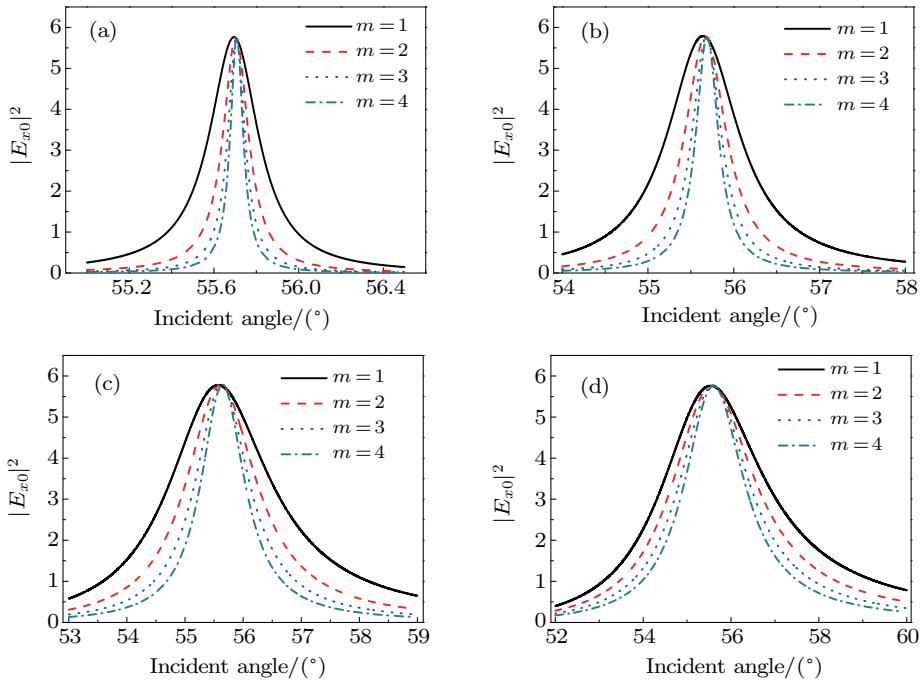



**Fig. 7.** (color online) Variations of $|E_{x0}|^2$ with incident angle for the SPR sensors with different-order ($m = 1, 2, 3, 4$) (a) NaCl, (b) MgO, (c) $TiO_2$, and (d) AlAs absentee layer.

#### 3.1.5. Electric field analysis

To investigate the origin of performance difference of SPR sensors with different-order absentee layer, the distributions of normalized tangential electric field intensity ($|E_x|^2$) of SPR sensors with different-order absentee layer are plotted in Fig. 6, using the calculation method described by Shalabney and Abdulhalim.[12] The SPR sensors with different-order NaCl, MgO, $TiO_2$ or AlAs absentee layer all exhibit different $|E_x|^2$ in their respective absentee layer, but show the same $|E_x|^2$ in metal layer and analyte, which is the reason for the same resonance angle and depth of dip. In addition, the SPR sensor with higher-order absentee layer exhibits larger propagation length of surface plasmon as shown in Fig. 6, which leads to sharper reflectance dip (smaller FWHM).[29]

The origin of the sensitivity decreasing with increasing $m$ is also studied by analyzing the electric field intensity. In Fig. 7, the normalized tangential electric field intensity at the analyte interface ($|E_{x0}|^2$) with the changing incident angle is plotted for the SPR sensors with different-order absentee layer. As $m$ increases, the integrals of $|E_{x0}|^2$ decreases obviously. This result confirms the statement of correlation between the sensitivity and the electric field integral.[27,30]

### 3.2. $S$, FWHM, and FOM versus refractive index of absentee layer

#### 3.2.1. $S$ versus $n_2$

Figure 8 shows the curves of sensitivity of the SPR sensor versus absentee layer refractive index ($n_2 = 1.5$–$5.0$) for various-order absentee layer ($m = 1, 2, 3, 4$). It is seen that the sensitivity increases with the increasing of the refractive index of absentee layer for different orders. But with the increasing of the order of absentee layer, the sensitivity decreases.

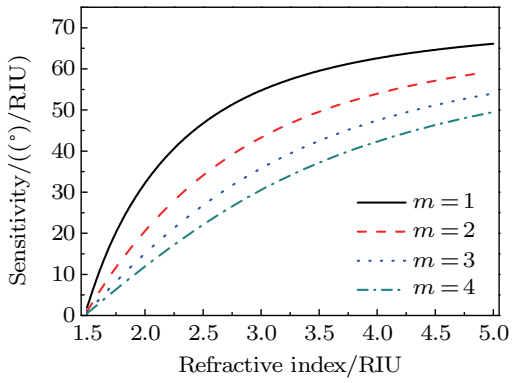



**Fig. 8.** (color online) Plots of sensitivity versus refractive index of absentee layer for $m = 1, 2, 3, 4$ respectively.

#### 3.2.2. FWHM versus $n_2$

Figure 9 exhibits the curves of FWHM of the SPR sensor with different absentee layer refractive index ($n_2 = 1.5$–$5.0$) for various-order absentee layer ($m = 1, 2, 3, 4$). As the refractive index of absentee layer increases or the order of absentee layer decreases, the FWHM also increases, which is similar to the case of the sensitivity.

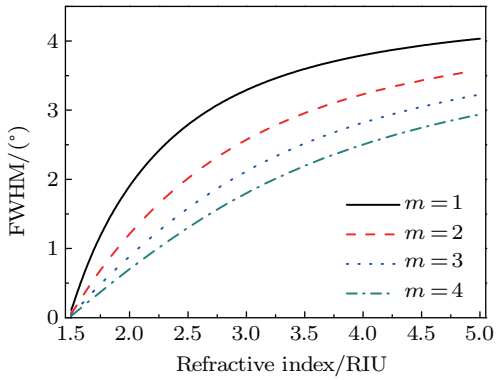



**Fig. 9.** (color online) Plots of FWHM versus refractive index of absentee layer for $m = 1, 2, 3, 4$ respectively.

#### 3.2.3. FOM versus $n_2$

Figure 10 shows that the curves of FOM of the SPR sensor versus absentee layer refractive index ($n_2 = 1.5$–$5$) for various order absentee layer ($m = 1, 2, 3, 4$). The result indicates that each FOM curve goes down with the increase of the refractive index of absentee layer. When the refractive index of absentee layer is bigger than 1.76 ($n_2 > 1.76$), the FOM of the SPR sensor increases with the increasing of $m$ as shown in Fig. 10. However, when $n_2 < 1.76$, the FOM decreases with the increasing of $m$ as shown in the inset of Fig. 10. This is the reason why FOM enhancement can only be achieved by using high-order $TiO_2$ or AlAs absentee layer, whose refractive index fulfills $n_2 > 1.76$. So, the FOM enhancement can be realized by using the high-order absentee layer with high refractive index.

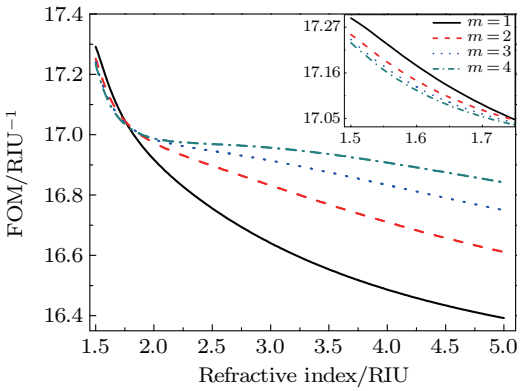



**Fig. 10.** (color online) Plots of FOM versus refractive index of absentee layer for $m = 1, 2, 3, 4$ respectively. The inset shows the linear amplification at low refractive index.

### 3.3. FOM versus $m$

To further investigate the FOM enhancement of the SPR sensor with high-order absentee layer, we study the FOMs of the SPR sensors with different-order $TiO_2$ and AlAs absentee layer as shown in Fig. 11. In Figs. 11(a) and 11(b), both FOM curves first go up rapidly with the increasing of $m$, and

then become flat, indicating that the FOM cannot increase indefinitely, but tends asymptotically towards a maximum value. When $m$ is large enough, the absentee layer is very thick. In this case, the absentee layer can be considered to be a semi-infinite medium, and the effect of its thickness (or $m$) on the performance of the sensor is insignificant, leading to nearly constant value of FOM. The maximum value of FOM for the SPR sensor with high-order $TiO_2$ (or AlAs) absentee layer is 16.987 (or 17.049) $RIU^{-1}$, which is 1.059% (or 2.587%) higher than the one with one-order absentee layer.

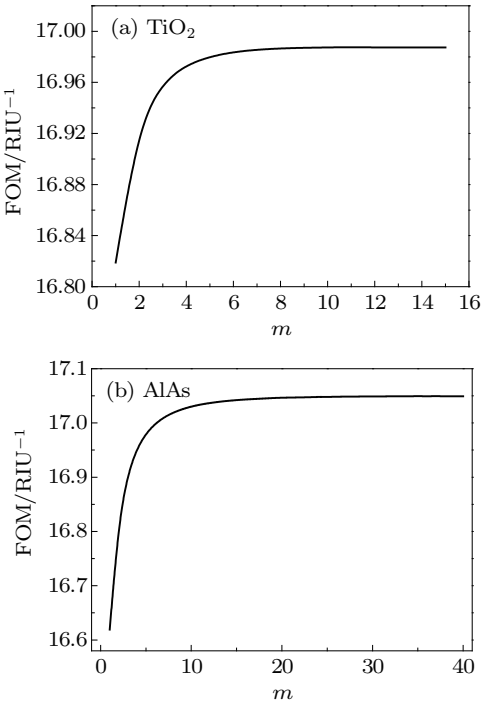



**Fig. 11.** Variations of FOM with the order of (a) $TiO_2$ and (b) AlAs absentee layer.

## 4. Concluding remarks

In this paper, the performance of the surface plasmon resonance sensor with high-order absentee layer is theoretically investigated. By analyzing the performance paramaters (sensitivity, FWHM and FOM) of SPR sensors with high-order absentee layer, we find that with the increasing of the order of absentee layer, the sensitivities and FWHMs of those SPR sensors both decrease, but the variation of FOM depends on the refractive index of absentee layer. To achieve FOM enhancement, only high-refractive-index absentee layer (such as $TiO_2$ or AlAs absentee layer) can be used. By investigating the FOM enhancement of the SPR sensor with high-order absentee layer, we also find the FOM cannot increase indefinitely with the increasing of the order of absentee layer, but tends asymptotically towards a maximum value. The maximum value of FOM for the SPR sensor with high-order $TiO_2$ (or AlAs) absentee layer is 1.059% (or 2.587%) higher than the one with one-order absentee layer.

## References

[1] Verma R, Gupta B D and Jha R 2011 *Sens. Actuators B* **160** 623
[2] Mohanty G, Akhtar J and Sahoo B K 2016 *Plasmonics* **11** 189
[3] Zhang Q Y, Zeng J, Li J F, Zhou Y B, Zhang X H and Cao H D 2014 *Acta Phys. Sin.* **63** 034207 (in Chinese)
[4] Chen L, Xu N N, Singh L, Cui T J, Singh R, Zhu Y M and Zhang W L 2017 *Adv. Opt. Mater.* **5** 1600960
[5] Chen L, Zhu Y M, Zhang D W, Cao Z Q and Zhuang S L 2009 *Chin. Phys. B* **18** 4875
[6] Chen L, Wei Y M, Zang X F, Zhu Y M and Zhuang S L 2016 *Sci. Rep.* **6** 27324
[7] Zhao X H, Su Y C, Tsai W H, Wang CH, Chuang T L, Lin C W, Tsao Y C and Wu M S 2015 *Opt. Commun.* **335** 32
[8] Das R, Srivastava T and Jha R 2015 *Sens. Actuators B* **206** 443
[9] Bao M, Li G, Jiang D M, Cheng W J and Ma X M 2012 *Appl. Phys. A* **107** 279
[10] Abbas A, Linman M J and Cheng Q 2011 *Sens. Actuators B* **156** 169
[11] Lan G Q, Liu S G, Ma Y, Zhang X R, Wang Y X and Song Y L 2015 *Opt. Commun.* **352** 49
[12] Shalabney A and Abdulhalim I 2010 *Sens. Actuators A* **159** 24
[13] Lahav A, Auslender M and Abdulhalim I 2008 *Opt. Lett.* **33** 2539
[14] Verma A, Prakash A and Tripathi R 2015 *Opt. Commun.* **357** 106
[15] Zhang Q Y, Zeng J, Li J F, Zhou Y B, Zhang X H and Cao H D 2014 *Acta Phys. Sin.* **63** 034207 (in Chinese)
[16] Ghosh S and Ray M 2014 *Sens. Actuators B* **205** 298
[17] Verma A, Prakash A and Tripathi R 2016 *Optik* **127** 1787
[18] Nenninger G G, Tobiška P, Homola J and Yee S S 2001 *Sens. Actuators B* **74** 145
[19] Shalabney A and Abdulhalim I 2012 *Opt. Lett.* **37** 1175
[20] Sang T, Wang Y K, Li J L, Zhou J Y, Jiang W W, Wang J C and Chen G Q 2017 *Opt. Commun.* **382** 138
[21] Shin D, Liu Z S and Magnusson R 2002 *Opt. Lett.* **27** 1288
[22] Chen Z Y, Zhao X, Lin C Y, Chen S J, Yin L and Ding Y C 2016 *Appl. Opt.* **55** 6832
[23] Wu W J, Zhu J T, Wang Z S, Zhang Z, Wang F L, Wang H C, Zhang S M, Xu Y, Cheng X S, Wang B, Li C X, Wu Y R, Qin S J, Chen L Y, Zhou H J and Huo T L 2006 *Chin. Phys. Lett.* **23** 2534
[24] Maharana P K, Jha R and Palei S 2014 *Sens. Actuators B* **190** 494
[25] Sharma N K, Yadav S and Sajal V 2014 *Opt. Commun.* **318** 74
[26] Palik E D 1998 *Handbook of optical constants of solids* (San Diego: Academic Press) pp. 775–793
[27] Benkabou F and Chikhi M 2014 *Phys. Status Solidi A* **211** 700
[28] Lahav A, Shalabaney A and Abdulhalim I 2009 *J. Nanophoton.* **3** 031501
[29] Matsubara K, Kawata S and Minami S 1990 *Opt. Lett.* **15** 75
[30] Shalabney A and Abdulhalim I 2011 *Laser Photon. Rev.* **5** 571